Visualising alloy fluctuations by spherical-aberration–corrected HRTEM

2010 EPL 91 36001

(http://iopscience.iop.org/0295-5075/91/3/36001)

A Letters Journal Exploring the Frontiers of Physics

August 2010

EPL, **91** (2010) 36001
doi: 10.1209/0295-5075/91/36001

www.epljournal.org

Visualising alloy fluctuations by spherical-aberration–corrected HRTEM

M. J. Casanove[(a)], N. Combe, F. Houdellier and M. J. Hÿtch

CNRS, CEMES (Centre d'Elaboration des Matériaux et d'Etudes Structurales) - BP 94347, 29 rue J. Marvig, F-31055 Toulouse, France, EU
Université de Toulouse, UPS - F-31055 Toulouse, France, EU

received 8 June 2010; accepted in final form 23 July 2010
published online 19 August 2010

PACS 68.55.Nq – Composition and phase identification
PACS 68.37.-d – Microscopy of surfaces, interfaces, and thin films
PACS 68.37.Og – High-resolution transmission electron microscopy (HRTEM)

Abstract – Under specific conditions of specimen thickness and experimental settings, aberration-corrected high-resolution transmission electron microscopy images of a SiGe alloy grown on a silicon substrate display strong intensity variation from one atomic column to the other. Combining TEM image processing, semi-empirical atomic simulations of large three-dimensional structures including the SiGe/Si interface and TEM image simulations, it is demonstrated that the observed contrast is strongly correlated to the Ge content in the different atomic columns. From a theoretical point of view, this reveals new possibilities for Cs-corrected transmission electron microscopy to observe chemical contrast, and more generally opens new routes for chemical mapping in nanoalloys.

Most techniques suitable for combining structural and chemical analyses of nanoalloys are likely to provide very accurate measurements of their mean composition and structure. However, except in ordered alloys in which the different elements are assigned to specific sites in the unit cell, the composition will vary from one atomic column to the other, as will the local bond lengths. As long as the probed volume remains large enough, such fluctuations are hardly observable since for a N-atom column, composition fluctuations typically scale as $1/\sqrt{N}$. When investigating nanoalloys (dots, particles or thin films), the local composition and in particular the presence of a compositional gradient can become a major issue, as they are likely to affect the desired properties. Up to now, most of the studies giving evidence for chemical contrast at the atomic scale have been focused on compounds, and not on alloys. Individual atoms of heavy elements have also been visualised by aberration-corrected scanning TEM in high-angle annular dark-field configuration (STEM-HAADF): Au on support films [1] and in nanowires of Si [2], dopant atoms of Sb in Si [3].

In this study, we demonstrate the possibility of distinguishing between two light atoms, Ge and Si, in the technologically important $Si_{0.7}Ge_{0.3}$ alloy using a high-resolution TEM fitted with a spherical-aberration corrector (Cs-corrected HRTEM) to optimize the contrast between the elements. The advent of Cs-correctors [4] has indeed provided new exciting ways for investigating materials at the atomic scale. Not only has the point resolution achievable in TEM been considerably improved for medium voltage machines and image delocalization effects minimized, but also the possibility of tuning experimental conditions, in particular Cs, has extended the spectrum of imaging modes [5,6].

For HRTEM observations at a zone axis, the atomic columns are composed of a finite, and indeed relatively small, number of atoms. The alloy fluctuations that we wish to investigate should produce observable contrast in the image. Because of the different parameters that can affect the contrast in TEM images, either due to experimental settings, specimen preparation (amorphous layers, vacancies, ...) or to static displacements [7] and strain, the experimental images have been compared with image simulations of large scale atomistic models.

A thin layer of $Si_{0.7}Ge_{0.3}$ was grown epitaxially on a silicon substrate by metal-organic chemical vapor deposition [8]. The cross-sections of the sample were cut along a (110) plane and thinned to electron transparency by

[(a)] E-mail: casanove@cemes.fr

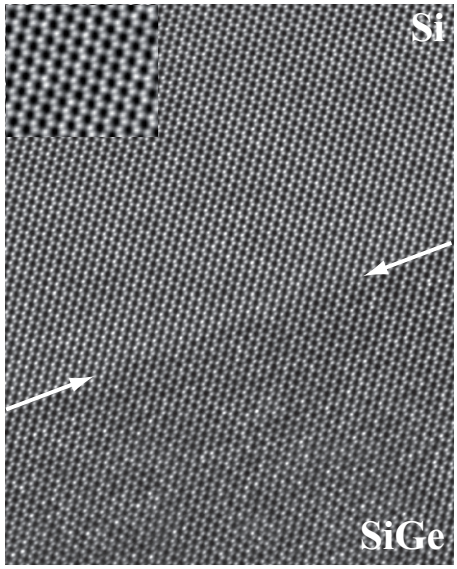

Fig. 1: HRTEM image of the $Si/Si_{0.7}Ge_{0.3}$ interface observed along a ⟨110⟩ zone axis. The interface is emphasized by the two white arrows. The inset shows a magnified region taken in the silicon part of the image and showing clearly the Si dumbbells which are displayed in bright contrast.

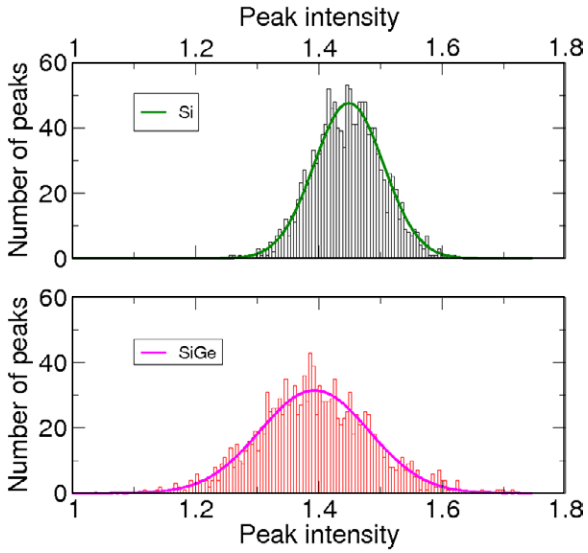

Fig. 2: (Colour on-line) Histograms of peak intensities established from 1340 peaks in Si and 1414 SiGe (above and below interface) and normalized with respect to the mean intensity in the analysed region of the image. For these Gaussian fits (solid lines), mean values and standard deviations are: in Si, mean = 1.448 and $\sigma = 0.078$; in SiGe, mean = 1.39 and $\sigma = 0.125$.

tripod polishing, a method which produces TEM specimens of well-defined geometry with minimal surface amorphous layers. TEM experiments were performed on the SACTEM-Toulouse [9], an FEI Tecnai F20 instrument operated at 200 kV fitted with a field emission gun and a CEOS spherical-aberration corrector. The point resolution of this instrument is 0.12 nm. Images were recorded on a 1k CCD camera (MSC Gatan) at a sampling density of 0.036 nm/pixels and analysed using in-house software. Atomistic modeling was performed using the Stillinger-Weber (SW) [10–13] semi-empirical potential for silicon and germanium. The choice of a semi-empirical potential is first justified by the large number of atoms (about 8000) to be considered. Moreover, the SW potential has been widely used for Si/Ge compounds [14,15], and produces realistic atomic structures with a degree of refinement well adapted to the present study [16].

Figure 1 presents a Cs-corrected image of the cross-sectional TEM specimen. Due to the difference in mean crystal potential on each side of the interface, the mean contrast looks darker in the SiGe side. However, an unexpected feature is observed: while the contrast in the Si substrate remains relatively constant, numerous bright dots stand out in the SiGe layer (referred to as "speckle" in the following). Such a difference is better assessed in the histograms of peak intensities in the corresponding regions, chosen at about 3 nm from the interface in order to avoid the localised effects of thin foil relaxation [17,18]. Note that in the present case, the ratio between the specimen thickness and the deposited $Si_{0.7}Ge_{0.3}$ layer ensures a uniform relaxation along the beam direction, except at the very interface. The histograms displayed in fig. 2 are fitted by Gaussian curves whose mean value and standard deviation are reported in the figure caption. Their analysis reveals that the standard deviation of peak intensity in the SiGe side is about 60% higher than in the Si side of the interface, which is significant and discloses the presence of speckle. Moreover, if we assume that the standard deviation in silicon results only from noise, and that this random noise level will be the same in the SiGe layer, the standard deviation of the speckle contrast in SiGe is as high as 0.098 (square root of the variance difference) *i.e.* 10% of the mean intensity.

Observing such contrast variations, or speckle, required specific experimental settings. First, the imaging conditions allowed us to distinguish the two different columns in the dumbbells (separated by only 0.14 nm). Then the atomic columns displayed bright contrast "white atoms". The point resolution achievable with the SACTEM-Toulouse is clearly sufficient to separate the different atomic columns but HRTEM images are well known to vary strongly with specimen thickness and defocus. We performed image simulations of a pure silicon thin film using the experimental settings of the microscope, and in particular a very weak Cs value of 1 μm. While HRTEM is clearly dominated by phase contrast, the choice of a very weak Cs value enables us to optimise the amplitude contrast, which proved essential for our purpose. Let us recall that such a setting can only be obtained thanks to the use of a Cs-corrector. The HRTEM image simulations were performed using the JEMS software, developed by Stadelmann [19]. Figure 3 presents the corresponding thickness-defocus map. Clearly, the silicon dumbbells

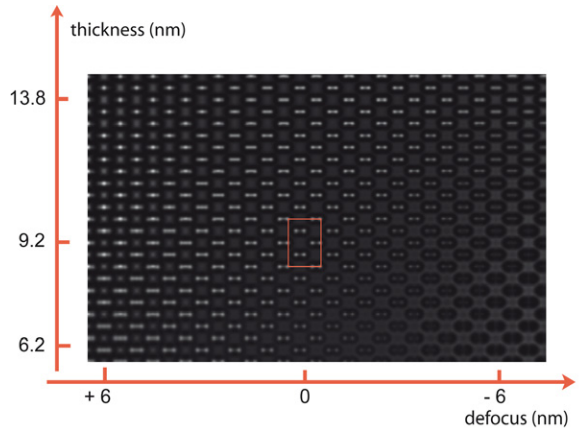

Fig. 3: (Colour on-line) Thickness-defocus map of silicon simulated HRTEM images observed along a [110] axis. Cs = 1 μm.

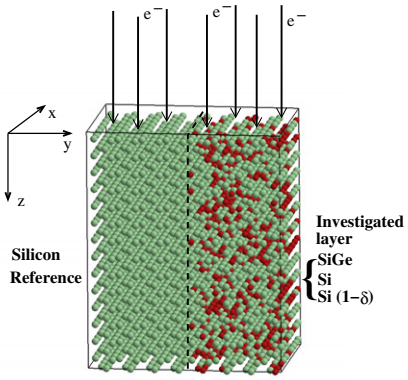

Fig. 4: (Colour on-line) Sketch of the super-cell probed by the electron beam. Periodic boundaries conditions are applied along the x and y directions.

are only observed in specific intervals of thickness and defocus. In particular, we see that the dumbbells are well separated in a thickness range going from 7 to 15 nm, at a defocus close to 0.

To find out the origin of the speckle in the SiGe layers, we identify several sources of image contrast: chemical composition (Si or Ge), atomic positions depending on the particular neighborhood (in SiGe), presence of vacancies and amorphous surface layers. Each of these sources is introduced in a separate atomistic model. Their incidence on the image contrast is then investigated through the analysis of HRTEM image simulations performed on these models. The atomistic models consist in a super-cell with dimensions (before optional relaxation) $12.3 \times 3.06 \times 4.34$ nm, including an interface separating a Si layer (to serve as reference) from a layer including the investigated sources: such procedure ensures the same imaging conditions on both sides of the simulated interface. Figure 4 sketches the super-cell probed by the electron beam. *Model Si/SiGe*: in the first model, all the atoms are positioned on the silicon crystal lattice but a random 30% of Si atoms

Table 1: Mean values and standard deviations taken from the histograms of peak intensities in the different simulated images for different thicknesses (normalized to the incident beam intensity).

Thickness (nm)	Model	Si reference		Layer	
		Mean	σ (%)	Mean	σ (%)
9.97	Si/SiGe	2.20	1.70	1.63	19.4
	Si/SiGe relaxed	2.28	2.98	1.68	20.7
	Si/Si relaxed	2.28	3.0	2.28	3.2
	Si/Si$(1-\delta)$ relaxed	2.28	3.2	2.30	6.3
	(Si/SiGe)+Am	2.189	6.88	1.622	20.4
8.43	Si/SiGe	2.01	1.55	1.59	25.3
7.67	Si/SiGe	1.844	1.6	1.505	25

are substituted by Ge atoms on one side of the interface. This model compares HRTEM image simulations intensities between a pure Si layer and a SiGe layer analysing the effect of the chemical composition. *Model Si/SiGe relaxed*: the second model is analogous to the first one but includes the relaxation of the unit cell and slight changes in the atomic positions depending on the particular neighborhood of the different atoms. Relaxation is performed by minimizing the total energy using a conjugated gradient algorithm. In addition, the unit cell is relaxed in the direction perpendicular to the interface in order to accommodate the in-plane compressive stress resulting from the lattice mismatch between the SiGe layer and the silicon substrate $\epsilon_{\parallel} = -1.2\%$. *Model Si/Si relaxed*: the effect of pure static displacements resulting from the lattice relaxation around Ge atoms was further analyzed by replacing the Ge atoms in the second model by silicon while keeping their position after relaxation. *Model* $Si/Si(1-\delta)$ *relaxed*: the fourth model analyzes the effect of a small amount of vacancies (5%). Vacancies are randomly distributed on one side of the interface in a Si crystal lattice and both cell and atomic positions are relaxed. *Model* $(Si/SiGe) + Am$: finally, in order to check the influence of noise, we added an amorphous carbon foil to the first model *i.e.* to both Si and SiGe layers. All the resulting super-cells were finally cut into slices perpendicular to the z-direction in order to provide models with different thickness from 0.77 nm to 12.3 nm for image simulations. Surprisingly, in the range of thickness suitable for obtaining a bright contrast in the atomic columns, the pure silicon columns remain the brighter. However, this is also the case in the experimental image.

We analyse the intensities of the different peaks (equivalent to atomic columns) on both sides of the interface for the relevant specimen thicknesses (cf. fig. 3) and in exactly the same way as for the experimental data. Peak histograms are fitted by a Gaussian distribution whose mean values and standard deviations are reported in the upper part of table 1 for a 9.97 nm thick specimen. The

variations of contrast in the Si reference substrate do not significantly depend on the model (except for the $Si/SiGe + Am$ model which include an additional noise), as expected, whereas significant standard deviations of peak intensities occur in the models involving Ge atoms. In particular, we do not observe any difference between the layer and the reference in the Si/Si *relaxed* model, which clearly implies that static displacements are not responsible for the speckle.

The $Si/Si(1-\delta)$ *relaxed* model exhibits a very weak contrast variation compared to the contrast induced by chemical composition. We therefore conclude from the upper part of table 1 that the observed speckle in fig. 1 originates from the chemical contrast of the Ge atoms.

We finally investigate the film thickness dependency on the results in the lower part of table 1. Variations of contrast in the SiGe layer are not significantly affected by the film thickness and thus does not alter our first conclusion. The enhancement of the relative speckle contrast is more due to the decrease in the mean intensities than the larger statistical variation in Ge-atom column composition for thinner samples.

The speckle contrast predicted by the simulations of about 20% (compared to the mean intensity) is twice the experimental value of about 10%. Some of this may be due to an inexactitude in the experimental conditions, notably thickness and crystal tilt, though the margin of error is small given that the dumbbell contrast is very sensitive to these parameters. We believe this more to be a manifestation of the "Stobbs" factor pertaining to a lower overall contrast in experimental images than in simulations [20]. An uniform background of diffuse intensity added to the simulations would produce a reduced relative speckle for example.

The HRTEM simulated images allow us to go beyond the bare analysis of peak histogram intensities since we know the exact composition of each atomic column. Indeed, there is a strong correlation between the image intensity of an atomic column and its Si content (and anti-correlation with Ge). Quantitative evidence of this correlation is provided by fig. 5 where the peak intensities in the HRTEM simulated image are plotted as a function of the silicon fraction in the corresponding atomic column. Whilst the dots corresponding to the silicon substrate are tightly gathered at the upper–right-hand corner of the figure, the dots corresponding to the SiGe layer are spread out. There are only 25 atoms in a column for this specimen thickness, so the Si fraction takes a range of values which correspond with a binomial distribution, as expected. It is interesting to note that for a particular Si fraction, there is a range of possible peak intensities. We interpret this as a result of the non-local nature of the HRTEM image contrast. Indeed, the intensity of a peak will be inevitably affected by the neighbouring columns, even for near-zero Cs imaging conditions. Besides, the exact distribution of the Si atoms within the column can also slightly change the corresponding peak intensity. The more remarkable

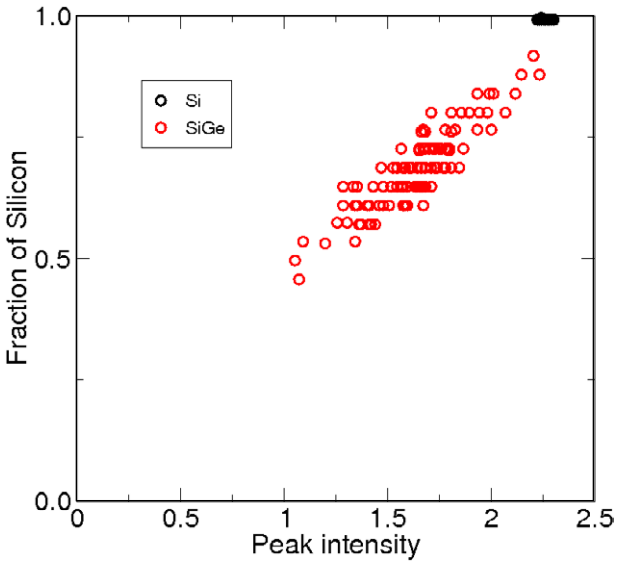

Fig. 5: (Colour on-line) *Model Si/SiGe relaxed*. Fraction of silicon in the atomic column as a function of the corresponding peak intensities in the HRTEM simulated image. Dots corresponding to the silicon substrate and to the SiGe layer are, respectively, reported in black and red. Film thickness = 9.97 nm, defocus = 0, Cs = 1 μm.

feature is the near-linear relationship between the silicon content and the simulated HRTEM peak intensity. These results should be related to the very particular imaging conditions that were used in the experiments, especially the use of a very small value of Cs and appropriate defocus. Note that with such conditions, the well-resolved atomic columns display bright contrast, the brighter corresponding to pure silicon columns, as verified both in the experimental image and the simulations.

In conclusion, we have been able to exhibit a speckle contrast in Cs-corrected HRTEM imaging of a Si/SiGe sample. Through the combination of atomic modelling and HRTEM image simulations, we have brought decisive evidence for the chemical composition origin of this speckle. Until now, aberration-corrected HRTEM has been used to detect individual self-interstitial atoms of Ge [21], the number of atoms in columns of Au [22] and the light element of oxygen in a perovskite [23]. Here, we succeeded in showing variations of two light elements within an alloy by emphasizing the amplitude contrast in aberration-corrected HRTEM. Remarkably, a linear relation between the chemical composition of an atomic column and its HRTEM image intensity has also been uncovered. The exploitation of this method implies both a detailed analysis of peak intensity histograms, such as the one displayed in fig. 2 and a reference for the peak intensities —in our case, the silicon layer. This reference must be free from dopants or vacancies and with the same thickness as the investigated doped region. We showed that the quantitative estimation of the silicon content of each atomic column is possible from the simulated TEM images

(fig. 5). Unfortunately, the experimental images have a continuous background, not taken into account in simulations, so that the ratio between the mean peak intensities in the reference and in the investigated region is not always reliable for a quantitative exploitation. This potential drawback could be reduced through further refinements of the image simulation theory combined with enhanced description of the experimental continuous background in the images. Beyond these difficulties, our results reveal a new method for localizing and quantifying atoms using unexpected capabilities of HRTEM. The extension of these results to a wider range of nanoalloys systems are under consideration.

* * *

This work has been supported by the French National Agency (ANR) in the frame of its programme in Nanosciences and Nanotechnologies (CARTODOP project ANR-06-NANO-046-06). The authors are grateful to L. Clément and J.-L. Rouvière (CEA-Grenoble) for supplying the TEM specimen.

REFERENCES

[1] Batson P., *Microsc. Microanal.*, **14** (2008) 89.
[2] Allen J., Hemesath E. R., Perea D. E., Lensch-Falk J. L., Li Z., Yin F., Gass M. H., Wang P., Bleloch A. L., Palmer R. E. and Lauhon L. J., *Nat. Nanotechnol.*, **3** (2008) 168.
[3] Voyles P. M., Muller D. A., Grazul J. L., Citrin P. H. and Gossman H.-J. L., *Nature*, **416** (2002) 826.
[4] Rose H., *Optik*, **85** (1990) 19.
[5] Haider M., Rose H., Uhlemann S., Schwan E., Kabius B. and Urban K., *Nature*, **392** (1998) 768.
[6] Lentzen M., Jahnen B., Jia C. L., Thust A., Tillman K. and Urban K., *Ultramicroscopy*, **92** (2002) 233.
[7] Glas F., *Phys. Rev. B*, **51** (1995) 825.
[8] Hartmann M., Loup V., Rolland G., Holliger P., Laugier F., Vannuffel C. and Séméria M. N., *J. Cryst. Growth*, **236** (2002) 10.
[9] Houdellier F., Hÿtch M., Hüe F. and Snoeck E., *Advances in Imaging and Electron Physics*, Vol. **153** (Elsevier, Amsterdam) 2008, Chapt. 6, pp. 1–36.
[10] Stillinger F. H. and Weber T. A., *Phys. Rev. B*, **31** (1985) 5262.
[11] Stillinger F. H. and Weber T. A., *Phys. Rev. B*, **33** (1986) 1451.
[12] Laradji M., Landau D. P. and Dünweg B., *Phys. Rev. B*, **51** (1995) 4894.
[13] Vink R., Barkema G., der Weg W. V. and Mousseau N., *J. Non-Cryst. Solids*, **282** (2001) 248.
[14] Nurminen L., Tavazza F., Landau D. P., Kuronen A. and Kaski K., *Phys. Rev. B*, **68** (2003) 085326.
[15] Hadjisavvas G. and Kelires P. C., *Phys. Rev. B*, **72** (2005) 075334.
[16] Nurminen L., Tavazza F., Landau D. P., Kuronen A. and Kaski K., *Phys. Rev. B*, **67** (2003) 035405.
[17] Treacy M. M., Gibson J. M. and Howie A., *Philos. Mag.*, **51** (1985) 389.
[18] Gatel C., Tang H., Crestou C., Ponchet A., Bertru N., Doré F. and Folliot H., *Acta Mater.*, **58** (2010) 3238.
[19] Stadelmann P., *Ultramicroscopy*, **21** (1987) 131.
[20] Hÿtch M. and Stobbs W., *Ultramicroscopy*, **53** (1994) 191.
[21] Alloyeau D., Freitag B., Dag S., Wang L. W. and Kisielowski C., *Phys. Rev. B*, **80** (2009) 014114.
[22] Kisielowski C., Freitag B., Bischoff M., van Lin H., Lazar S., Knippels G., Iemeijer P. T., van der Stam M., von Harrach S., Stekelenburg M., Haider M., Uhlemann S., Müller H., Hartel P., Kabius B., Miller D., Petrov I., Olson E., Donchev T., Kenik E., Lupini A., Bentley J., Pennycook S., Anderson I., Minor A., Schmid A., Duden T., Radmilovic V., Ramasse Q., Watanabe M., Erni R., Stach E., Denes P. and Dahmen U., *Microsc. Microanal.*, **14** (2008) 469.
[23] Jia C. L., Lentzen M. and Urban K., *Science*, **299** (2003) 870.